

Improvement of 3D mean field models for capillarity-driven grain growth based on full field simulations

**L. Maire, B. Scholtes, C. Moussa,
N. Bozzolo, D. Pino Muñoz &
M. Bernacki**

Journal of Materials Science

Full Set - Includes 'Journal of Materials
Science Letters'

ISSN 0022-2461

Volume 51

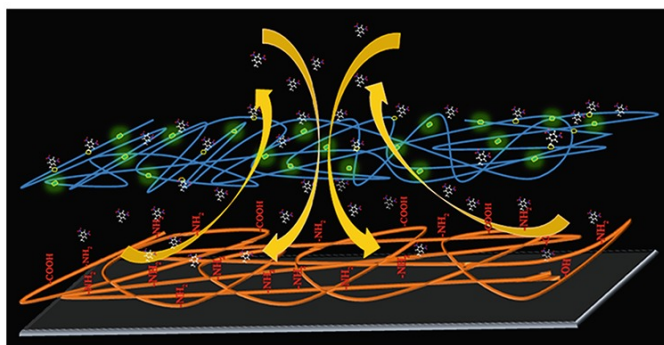
Number 24

J Mater Sci (2016) 51:10970-10981

DOI 10.1007/s10853-016-0309-6

Volume 51 • Number 24
December 2016

Journal of Materials Science



jms

10853 • 51(24) 10663–11038 (2016)
ISSN 0022-2461 (Print)
ISSN 1573-4803 (Electronic)

 Springer

 Springer

Your article is protected by copyright and all rights are held exclusively by Springer Science +Business Media New York. This e-offprint is for personal use only and shall not be self-archived in electronic repositories. If you wish to self-archive your article, please use the accepted manuscript version for posting on your own website. You may further deposit the accepted manuscript version in any repository, provided it is only made publicly available 12 months after official publication or later and provided acknowledgement is given to the original source of publication and a link is inserted to the published article on Springer's website. The link must be accompanied by the following text: "The final publication is available at link.springer.com".



Improvement of 3D mean field models for capillarity-driven grain growth based on full field simulations

L. Maire^{1,*}, B. Scholtes¹, C. Moussa¹, N. Bozzolo¹, D. Pino Muñoz¹, and M. Bernacki¹

¹MINES ParisTech, PSL - Research University, CEMEF - Centre de mise en forme des matériaux, CNRS UMR 7635, CS 10207 rue Claude Daunesse, 06904 Sophia Antipolis Cedex, France

Received: 18 June 2016

Accepted: 16 August 2016

Published online:
31 August 2016

© Springer Science+Business
Media New York 2016

ABSTRACT

In the present study, mean field models of grain growth (Hillert and Burke–Turnbull models) are compared with 3D full field simulations considering an isotropic grain boundary energy and mobility and under the absence of second-phase particles. The present 3D full field simulations are based on a level set description of the grain interfaces within a finite element framework. The digital initial microstructures are generated using a coupled “Voronoi–Laguerre/dense sphere packing” algorithm. Based on full field simulation results, new formulations of Burke–Turnbull and Hillert models are proposed. In contrast with classical formulations, the new ones account for the possible heterogeneity of the initial grain size distribution.

Introduction

Metallurgists have long observed that the macroscopic properties of the material, such as ductility, strength, thermal conductivity, and hardness are strongly related to the microstructure, and especially to the mean grain size $\langle R \rangle$. Thus, understanding the phenomenon of grain growth (GG) occurring after recrystallization is crucial for the optimization of the microstructure and the final in-use properties of the material.

Single-phase fully dense polycrystals can generally be described by a log-normal grain size distribution (GSD) [1–3], defined by $\langle R \rangle$ and a standard deviation (σ). The standard deviation is related to the width of the grain radius dispersion around $\langle R \rangle$. During grain growth mechanism, grain boundaries migrate under

capillarity effects which results in an increase of $\langle R \rangle$ and σ . A previous study has highlighted that the heterogeneity in terms of GSD in the microstructure at the early stages of grain growth may have a first-order influence on the overall kinetics [4], but this work was only based on 2D considerations.

Macroscopic models, also called *mean field* (MF) models, are widely used to describe the grain growth kinetics, mainly due to their low computational cost. These models are based on empirical or semi-empirical laws and require experimental investigations to calibrate fitting parameters. Furthermore, given that these models are most of the time based on average fields (mean radius and mean curvature), they are not adapted for capturing heterogeneous phenomena such as abnormal grain growth.

Address correspondence to E-mail: ludovic.maire@mines-paristech.fr

Table 1 Characteristics of the initial (lines 1–4) and final (lines 5–8) GSDs predicted by the full field simulations

	LN ₁	LN ₂	LN ₃	LN ₄	LN ₅	LN ₆	LN ₇	BiM
Initial state ($t = 0$ h)								
$\langle R_0 \rangle$ (μm)	62.0	66.0	74.3	75.3	82.2	89.4	99.0	75.2
σ_0 (μm)	6.90	11.8	19.4	7.50	25.9	30.9	17.7	25.5
$\ln(\sigma_0/\langle R_0 \rangle)$	-2.20	-1.71	-1.35	-2.30	-1.14	-1.05	-1.71	-1.08
No. grains	7920	7576	7474	8100	7460	7636	7588	7472
Final state ($t = 5$ h)								
$\langle R_f \rangle$ (μm)	109	120	135	111	151	160	138	115
σ_f (μm)	39.0	45.0	53.2	39.8	59.9	66.3	50.7	36.0
$\ln(\sigma_f/\langle R_f \rangle)$	-1.03	-0.98	-0.93	-1.03	-0.92	-0.88	-1.00	-1.16
No. grains	1483	1278	1244	2552	1221	1341	2803	2092

Thanks to the increase in computer performances, finer approaches called *full field* (FF) models have emerged in the last decades. These approaches consider a complete description of the microstructure topology at the polycrystal scale. A review of the most significant numerical methods is given in [5]. Probabilistic voxel-based approaches such as *Monte Carlo* [6–8] and *cellular automata* [9] are very popular. Another approaches found in the literature is the *phase-field* [10] method, which offers the advantage of avoiding the difficult problem of tracking the interfaces. Finally, grain growth can also be modeled using a *level set* description of the interfaces within a finite element framework [11–14], which is the full field method used in this work.

In this study, we propose to quantify the influence of the initial GSD in the context of 3D grain growth. More specifically, the predictions of the Hillert [15] and Burke–Turnbull (B&T) [16] grain growth models are confronted with full field numerical simulations at the scale of a representative elementary volume (REV) and under the assumptions of isotropic grain boundary energy and mobility, constant temperature, and no precipitates. The digital initial microstructures are generated using a coupled “Voronoi–Laguerre/dense sphere packing” algorithm [17, 18].

Full field modeling of grain growth

Material parameters and numerical tools

A 5-h heat treatment at a constant temperature of 1050 °C for the austenitic 304L steel is simulated. Isotropic values are considered for the grain boundary mobility (M) and energy (γ). More precisely the product $M\gamma$ is fixed to 8.28×10^{-7} J mm⁻², which is

representative of a 304L stainless steel at 1050 °C [4, 19]. The material is assumed to be free of second-phase particles (no Zener pinning effect).

The numerical simulations are performed on a cubic REV whose edge length varies from 2.00 to 2.85 mm. Each simulation was performed on 60 Intel Xeon CPUs. An unstructured mesh composed of 292³ tetrahedral elements is used.

Eight different initial GSDs are considered to generate eight initial digital polycrystals. Each of them is defined by an initial mean grain radius $\langle R_0 \rangle$ and standard deviation σ_0 . Their characteristics are summarized in Table 1 (line 1–4). The distributions LN _{i} with $i \in \{1, \dots, 7\}$ follow a log-normal distribution. The last one, referred to as BiM, is bimodal with modes $\lambda_1 = 50 \mu\text{m}$ and $\lambda_2 = 100 \mu\text{m}$. The initial number of grains in the REV is close to 8000, while at least 1200 grains remain at the end of the heat treatment (see Table 1). The REV dimensions, the time step and the mesh size are chosen so as to justify a good convergence of results in terms of grain boundary kinetics [13, 20].

Full field simulation results

A histogram representing the instantaneous GSD is generated every minute of the heat treatment simulation. Each histogram is composed of 30 equally spaced intervals delimited by 0 and 300 μm . Next, the term *distribution curve* is introduced to denote a linear approximation of a GSD histogram. The objective of these distribution curves is to simplify the representation of the GSDs for future comparisons. Figure 1 provides a schematic illustration of the distribution curve obtained by piecewise linear approximation of a histogram.

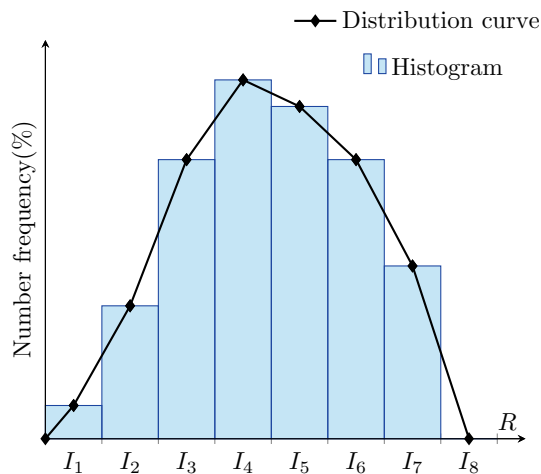


Figure 1 Distribution curve obtained by linear approximation of a histogram.

Figure 2 shows all the distribution curves predicted by the full field simulations for every initial GSDs at the early (solid curves) and final (dashed curves) stages of the simulation. These will be confronted with the Hillert model predictions in the next section.

Table 1 (line 5–8) presents the characteristics of the final GSDs predicted by the full field simulations. The ratio $\ln(\sigma_f/\langle R_f \rangle)$ is observed to tend toward the value -1.00 after 5 h of treatment for every initial GSD. Figure 3 illustrates several REV of full field simulations at the beginning and at the end of the heat treatment, for the LN_1 and BiM initial GSDs. Among the REV representing the log-normal GSDs, only the REV obtained for the LN_1 initial GSD is depicted since this latter is representative of all the log-normal initial GSDs. A preponderant blue color is observed at the beginning of the heat treatment for the LN_1 initial GSD, meaning that σ_0 is small for this distribution and most grains have sizes close to $\langle R_0 \rangle$. In the BiM initial GSD, two preponderant blue and green colors are observed in the REV at the beginning of the heat treatment. These two colors depict the two modes of the bimodal distribution, centered on grain size values of 50 and 100 μm .

Confrontations of full field simulation results with Hillert model

Hillert model

In 1965, Hillert proposed a mean field model [15] for normal grain growth. This model has already been

discussed in many studies. Several authors, as in [21–24], recently confronted the predictions of this model with full field simulation results. Hillert model is considered to be more accurate than other grain growth models such as the one of B&T [16], since it is based on a discrete representation of the microstructure. This discrete microstructure is composed of N classes of spherical grains having a radius R_i ($i \in \{1, \dots, N\}$). Each class of grains evolves according to the following equation:

$$\dot{R}_i = \beta M \gamma \left(\frac{1}{R_{cr}} - \frac{1}{R_i} \right), \quad (1)$$

where \dot{R}_i is the time derivative of R_i and R_{cr} is a critical grain radius. By applying the volume conservation in 3D, it can be demonstrated that $R_{cr} = \langle R^2 \rangle / \langle R \rangle$ [22, 24, 25]. For each initial GSD, the number of classes in the Hillert model has been taken equal to the number of grains in the REV of the corresponding full field simulation (see Table 1). The parameter β is a geometrical dimensionless constant which refers to the inherent approximations concerning the assumed idealized geometry in the Hillert model representation. In 3D, β is assumed to be close to unity [15]. Other authors have nevertheless reported values above unity, such as $\beta \simeq 1.25$ [21] and $\beta \simeq 1.1$ [23]. In [22], the authors recently discussed a linear relationship valid in 3D between the parameter β and the index $\langle R \rangle^2 / \langle R^2 \rangle$ which aims to account for the geometrical relations between the neighborhood grains for any given initial distribution.

Hereafter, the notation $Hi(\beta)$ designates Eq. 1. So $Hi(1)$ corresponds to the classical Hillert formulation [15]. As it employs several grain classes, this model has the advantage of being able to predict the GSD evolution in addition to the $\langle R \rangle$ evolution. Previous works have shown the ability of the classical Hillert model to correctly capture the grain growth kinetics in 2D for different initial GSDs [4]. In the same manner as for full field simulations, a GSD histogram is generated every minute of the Hillert simulation. The distribution curves are then deduced from the GSD histograms according to the method illustrated in Fig. 1.

The notation L_{Hi}^2 represents the instantaneous L^2 relative error measured between the distribution curves predicted by the Hillert and full field models. This quantity is computed as follows:

Figure 2 Initial (solid curves) and final (dashed curves) distribution curves predicted by the full field simulations for the different initial GSDs.

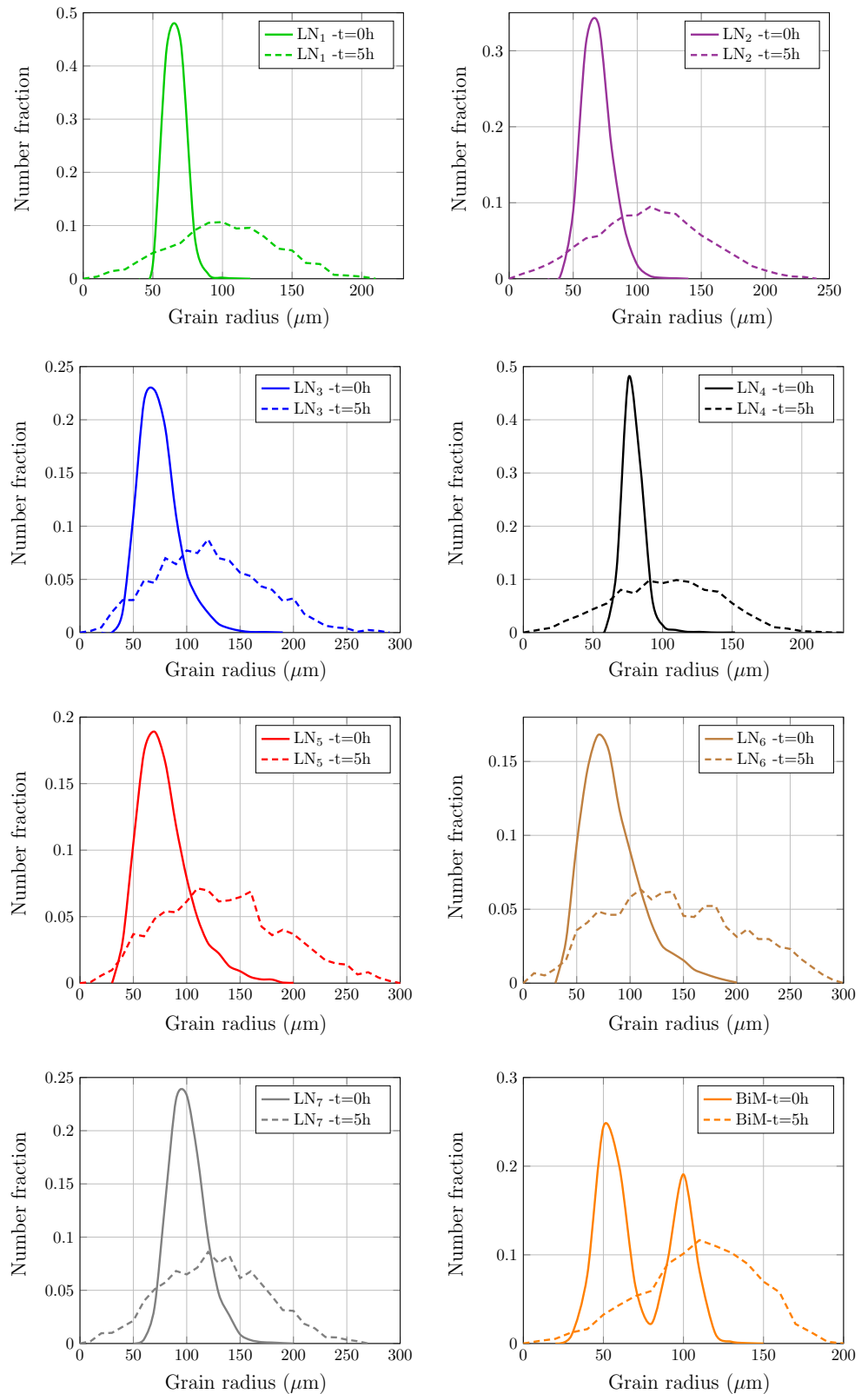
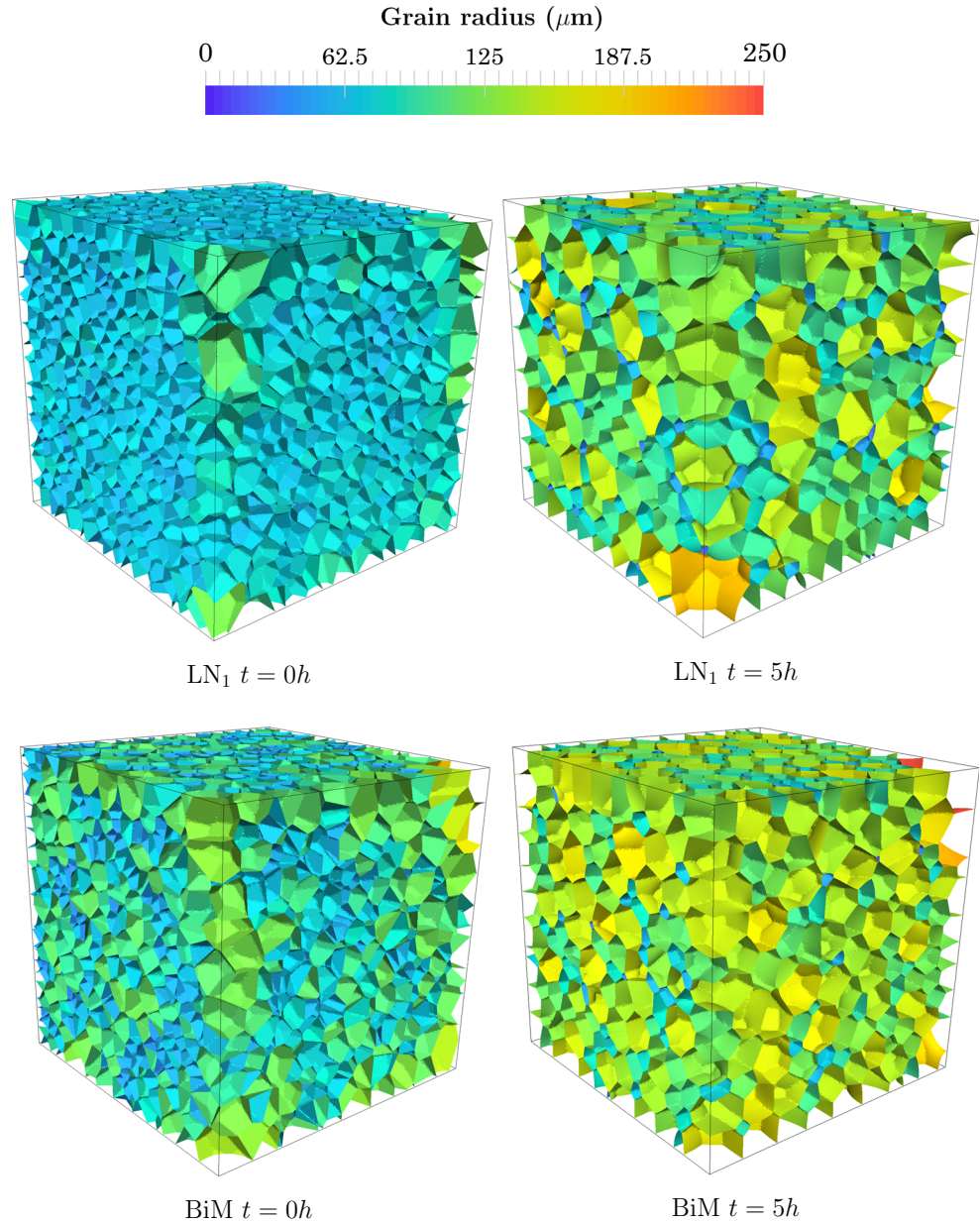


Figure 3 Grain boundary networks at initial and final stages of the simulation for the LN₁ and BiM initial GSDs. The color code corresponds to the equivalent sphere radius of each grain.



$$L_{\text{Hi}}^2(t) = 100 \times \sqrt{\frac{\sum_{i=1}^N (S_i - S'_i)^2}{\sum_{i=1}^N (S'_i)^2}}, \quad (2)$$

where, as illustrated in Fig. 4, the distributions are approximated by a linear interpolation and S_i (resp. S'_i) denotes the area of the i -th obtained trapezoid under the Hillert (resp. the full field) distribution curve. Hereafter, the notation $\langle L_{\text{Hi}}^2 \rangle$ designates the time average of the $L_{\text{Hi}}^2(t)$ errors for a given simulation:

$$\langle L_{\text{Hi}}^2 \rangle = \frac{1}{N_{\text{incr}}} \sum L_{\text{Hi}}^2(t), \quad (3)$$

where N_{incr} is the number of time increments (equal to 300 in this study, $dt = 1$ min).

Optimization of the Hillert model

The values of $\langle L_{\text{Hi}}^2 \rangle$ errors obtained with the Hi(1) model are depicted by blue bars in Fig. 5. This error remains globally constant around 20 % for all the initial GSDs. These results confirm the versatility of this model although a difference of 26 % is observed

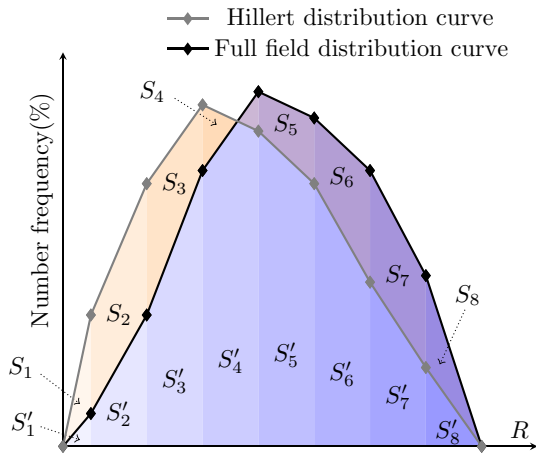


Figure 4 Computed L^2_{Hi} error between the Hillert and full field distribution curve.

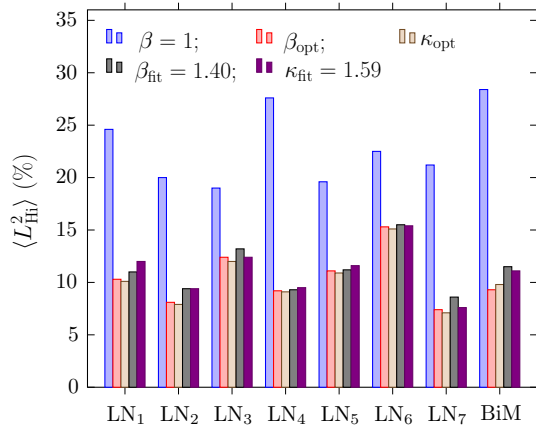


Figure 5 Comparison in terms of $\langle L^2 \rangle$ error on the distribution curves predicted by the full field and Hillert models (see Eq. 2 for details).

for the LN₄ and BiM initial GSDs. The distribution curves predicted by the Hi(1) (blue curves) and the FF model (red curves) are also compared at different

stages of the heat treatment in Fig. 7. The kinetic of grain growth obtained with the Hillert model seems to be slower than that obtained with the FF model. This is observable in Fig. 7 at each instant of the simulation by a time shift of the Hillert distribution curves with respect to the full field distribution curves.

As stated above, the value $\beta = 1$ proposed by Hillert relies on many assumptions. For example Hillert considers that each shrinking grain has four immediate neighbors just before disappearing. Furthermore, he considered that the β value is two times larger in 3D than in 2D where $\beta = 0.5$ according to Hillert [15]. Although these assumptions are judicious and justified, we propose to recalibrate this Hillert parameter based on the results of the full field simulations. Thus, several Hillert calculations have been performed by varying the β value from 0.5 to 2 by step of 0.01. We denote β_{opt} the value of β in Eq. 1 that minimizes $\langle L^2_{Hi} \rangle$ error for each initial GSD. The values of β_{opt} are provided in Table 2. Red bars in Fig. 5 show the residual $\langle L^2_{Hi} \rangle$ error obtained with β_{opt} . These residual errors have approximately been reduced by half compared to the classical value of β equal to 1. Furthermore, the values of β_{opt} are distributed around a mean value of 1.40 noted β_{fit} (see green dots in Fig. 6).

To validate the calibrated value of $\beta = 1.40$, the distribution curves predicted by the Hi(1.40) (green curves) and the full field models (red curves) are compared at different stages of the heat treatment in Fig. 7. It is worth noting that Hi(1.40) model provides non-negligible improvements for the prediction of the GSDs compared to the initial Hi(1) model. Indeed, the time shift observed in Fig. 7 between full field and Hi(1) distribution curves has been now rectified since this new value of $\beta = 1.4$ is larger than

Table 2 Line 1–2 Optimized Hillert model parameter β_{opt} calculated by inverse analysis from the full field simulation results (see Eq. 1) and fitted Hillert model parameter β_{fit} obtained by averaging the values of β_{opt}

	LN ₁	LN ₂	LN ₃	LN ₄	LN ₅	LN ₆	LN ₇	BiM
β_{opt}	1.32	1.32	1.28	1.43	1.41	1.39	1.52	1.53
β_{fit}				1.40				
κ_0	1.35	1.36	1.38	1.43	1.57	1.58	1.57	1.72
κ_{opt}	1.48	1.47	1.53	1.53	1.67	1.63	1.69	1.7
κ_{fit}				1.59				

Line 3 Values of κ_0 defined as the ratio between β_{opt} and the initial index $\langle R \rangle^2 / \langle R^2 \rangle$ at time = 0 s of every simulation. Line 4–5 Optimized κ values (κ_{opt}) calculated by inverse analysis from the full field simulation results (see Eq. 5) and fitted κ value (κ_{fit}) obtained by averaging the values of κ_{opt}

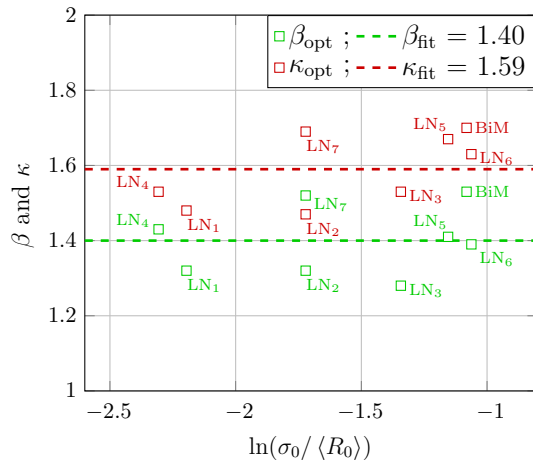


Figure 6 Optimized values β_{opt} and κ_{opt} obtained by inverse analysis from the FF simulation results and fitting values β_{fit} and κ_{fit} obtained by an average of the optimized values.

the old one and thus logically increases the kinetic of grain growth. In a general way, the shapes of the GSDs are also in good agreement with the observations detailed in [21]. GSDs are observed to be initially sharp and then become larger and larger during the heat treatment. After 2.5 h of treatment in the BiM initial case, one single peak is observed on the distribution curve, which means that the two modes merge in the first hours of the heat treatment.

In order to investigate further the theory of [22], we define κ_0 as

$$\kappa_0 = \frac{\beta_{opt}}{\langle R \rangle^2 / \langle R^2 \rangle_{(t=0)}}, \tag{4}$$

where the index $\langle R \rangle^2 / \langle R^2 \rangle$ is taken at the instant $t = 0$ s of the treatment. This choice has been done since this value does not significantly evolve during a simulation. The different values of κ_0 computed for every initial GSDs are provided in Line 3 of Table 2. These ratios are not constant between each initial GSDs, meaning that there is not a direct relation between β and the index $\langle R \rangle^2 / \langle R^2 \rangle_{(t=0)}$ for our cases. However this index, which considers the geometrical characteristics of neighboring grains, could be useful to enrich the classical Hillert model (see Eq. 1).

Thus by replacing the β parameter in Eq. 1 by the product of an assumed constant parameter noted κ times the ratio $\langle R \rangle^2 / \langle R^2 \rangle$, we can consider the following Hillert model derived from the Darvishi Kamachali theory [22]:

$$\dot{R}_i = \kappa \frac{\langle R \rangle^2}{\langle R^2 \rangle} M \gamma \left(\frac{1}{R_{cr}} - \frac{1}{R_i} \right), \tag{5}$$

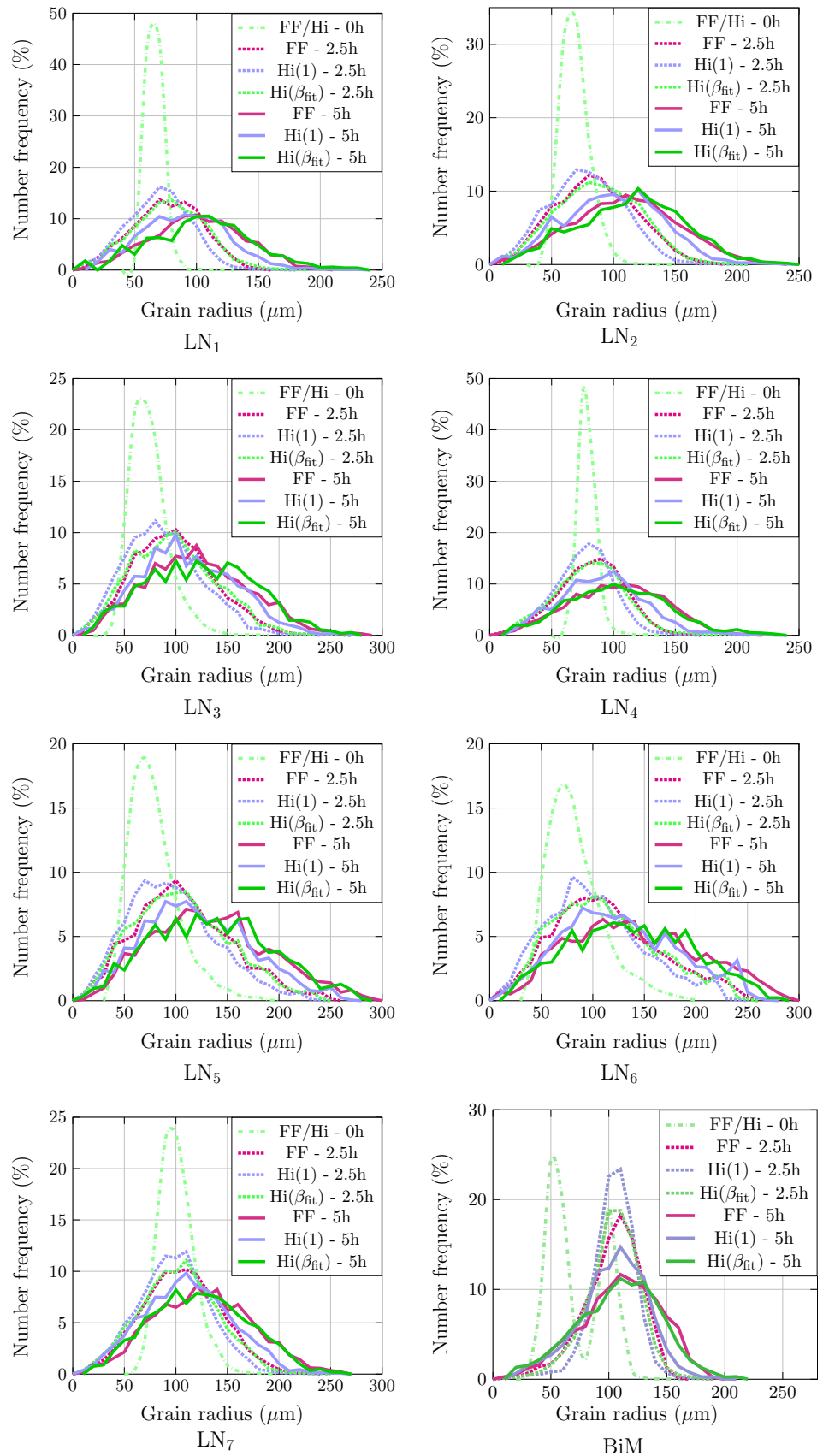
where κ is a constant parameter. We performed several Hillert calculations using this new formulation (see Eq. 5) and by varying the κ value from 1 to 2 with a step of 0.01. We denote by κ_{opt} the value of κ that minimizes $\langle L_{Hi}^2 \rangle$ for each initial GSD. The κ_{opt} values are presented in Line 4 of Table 2. Gray bars in Fig. 5 show the residual $\langle L_{Hi}^2 \rangle$ error obtained with κ_{opt} . These residual errors are slightly little smaller than those obtained with β_{opt} . However, this difference is not significant enough to affirm that the model given by Eq. 5 gives better predictions than Hi(1.4) model. Furthermore, the κ_{opt} values are distributed around a mean value of 1.59 noted κ_{fit} (see red dots in Fig.6) resulting also in a low $\langle L_{Hi}^2 \rangle$ error close to that obtained with the Hi(β_{fit}) model (see purple bars in Fig. 5). These similar errors are logically due to the fact that the Hi(1.4) (Eq. 1) and the new Hillert formulation (Eq. 5) give very close predictions since the index $\langle R \rangle^2 / \langle R^2 \rangle$ does not change much during all our simulations. Finally, the distributions curves obtained according to the new Hillert formulation all overlay with those obtained according to the Hi(1.4) model.

Confrontations of full field simulation results with B&T model

B&T model

For materials with a single-mode and uniform grain size, describing the evolution of $\langle R \rangle$ could be sufficient as this quantity determines the global mechanical behavior of the material. Especially, the Hall–Petch relationship states that the Yield stress of metallic materials can be expressed as a function of $\langle R \rangle^{-0.5}$ [26]. Furthermore in such cases, the initial GSD can be unknown and consequently the Hillert model can hardly be used. Thus, other mean field models can be used as a good alternative to describe the grain growth kinetics. In 1952, Burke and Turnbull (B&T) investigated the physical mechanisms of grain growth. They particularly assumed that grain boundaries migrate by atom transport toward their center of curvature, under a force due to their curved

Figure 7 Distribution curves predicted by the full field, Hi(1), and Hi(1.40) models for the different initial GSDs.



shape. These findings gave rise to the B&T model [16], which predicts a parabolic evolution of $\langle R \rangle$ as a function of the time t :

$$\langle R \rangle^2 - \langle R_0 \rangle^2 = \delta M \gamma t, \tag{6}$$

where $\delta = 0.5$ according to [16, 21]. This analytic mean field model has the advantage of being extremely simple to use since it requires only a value for the product $(M\gamma)$ and for the initial mean grain size $\langle R_0 \rangle$.

The predictions of the B&T model will be confronted with the full field simulation results, using the following relative L^2 error:

$$L_{B\&T}^2(\%) = 100 \times \sqrt{\frac{\sum_{t=0}^{5h} (\langle R \rangle_{FF}(t) - \langle R \rangle_{B\&T}(t))^2}{\sum_{t=0}^{5h} \langle R \rangle_{FF}^2(t)}}, \tag{7}$$

where $\langle R \rangle_{B\&T}$ and $\langle R \rangle_{FF}$ represent, respectively, the instantaneous values of $\langle R \rangle$ in the B&T and full field models.

New formulation of the B&T model

The resulting $L_{B\&T}^2$ measured between the classical B&T model predictions (Eq. 6) and the full field simulation results are illustrated by blue bars in Fig. 8. It is worth noting that these $L_{B\&T}^2$ are smaller than the $\langle L_{Hi}^2 \rangle$ calculated in the previous section. Indeed, $L_{B\&T}^2$ relies on a single quantity which is the mean grain size of the material. On the other hand,

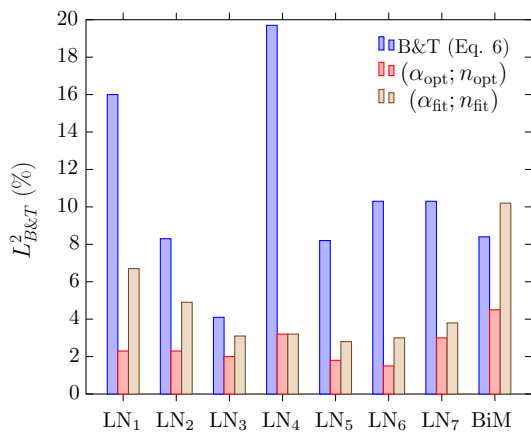


Figure 8 Comparison in terms of L^2 error on the $\langle R \rangle$ values predicted by the full field simulations and the different B&T formulations (see Eqs. 6 and 8 for more details).

$\langle L_{Hi}^2 \rangle$ reflects the difference of shape between the two distribution curves. Results show that $L_{B\&T}^2$ is globally high for any initial case. Furthermore, $L_{B\&T}^2$ error globally increases when the ratio $\sigma_0/\langle R_0 \rangle$ decreases. This finding is actually quite logical and can be easily explained. Indeed in the case of small $\sigma_0/\langle R_0 \rangle$ ratios, the grain boundary kinetic slows down at the early stages of the treatment because most grains have a initial radius close to $\langle R \rangle$. Consequently, the increase of $\langle R \rangle$ takes longer to initiate and a plateau or even a decrease could be observed at the beginning of the thermal treatment. These typical evolutions occurring during the transient regime are not straightforward to capture with the classical B&T model. Furthermore, given that the transient regime can last few hours in some initial configurations, it cannot be neglected by the models. These results confirm the interest of improving the classical B&T model. Recent numerical investigations in 2D have also pointed out that B&T model is not accurate for every $\sigma_0/\langle R_0 \rangle$ initial ratios [4].

In order to make the classical B&T formulation more accurate, the first objective is to determine whether there exist for each initial GSD, other δ values, noted δ_{opt} , that correctly describe the grain growth kinetics. These δ_{opt} values are obtained by minimizing the $L_{B\&T}^2$ for each initial GSD. The resulting fitting curves obtained by combining Eq. 6 and the δ_{opt} are depicted in Fig. 9 (dashed curves) for the LN₄ and LN₆ initial GSDs, which present the smallest and highest $\sigma_0/\langle R_0 \rangle$ ratios, respectively. It is observed that changing the values of δ does not correct the description of the transient regime. In particular for small $\sigma_0/\langle R_0 \rangle$ ratios, a model such as B&T model cannot be accurate enough to describe these particular mean grain size evolutions.

In order to also check the consistency of this law in the steady-state regime, the curves $\log(\langle R \rangle^2 - \langle R_0 \rangle^2) = f(\log(t))$ have been plotted in Fig. 10 according to full field results. A linear approximation of these curves is also added. We observed that the slopes of the linear approximations are quiet different for every initial GSD as already observed in the work of [4], which means that the classical B&T formulation cannot be sufficient to describe the kinetic of grain growth for every initial GSD.

Based on the previous observations, a new formulation of the B&T model has been proposed in [4] including a new fitting exponent n aiming to take into

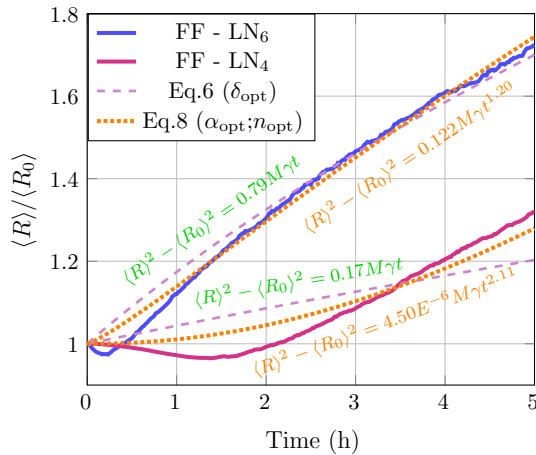


Figure 9 Evolution of $\langle R \rangle / \langle R_0 \rangle$ during the heat treatment. Solid curves correspond to the full field results, dashed curves represent the B&T predictions obtained by combining Eq. 6 and δ_{opt} , and dotted curves represent the B&T predictions obtained by combining Eq. 8 and the couple $(\alpha_{opt}; n_{opt})$.

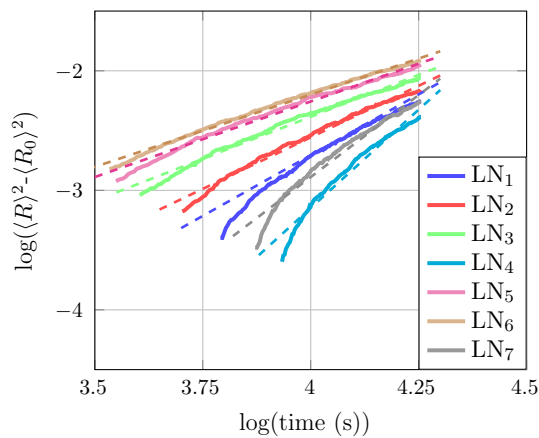


Figure 10 Evolution of $\log(\langle R \rangle^2 - \langle R_0 \rangle^2)$ as a function of $\log(t)$ during the steady-state regimes according to full field results. Linear approximations are added in dashed line.

account the different slopes observed in Fig. 10 and the transient regimes observed in Fig. 9:

$$\langle R \rangle^2 - \langle R_0 \rangle^2 = \alpha M \gamma t^n, \tag{8}$$

where α is considered as a fitting parameter depending, in the same manner as the exponent n , on the initial GSD characteristics. Thus, the validity of the classical B&T model (see Eq. (6)) can be easily verified if the slope n is equal to 1 and the fitted parameter α is equal to 0.5.

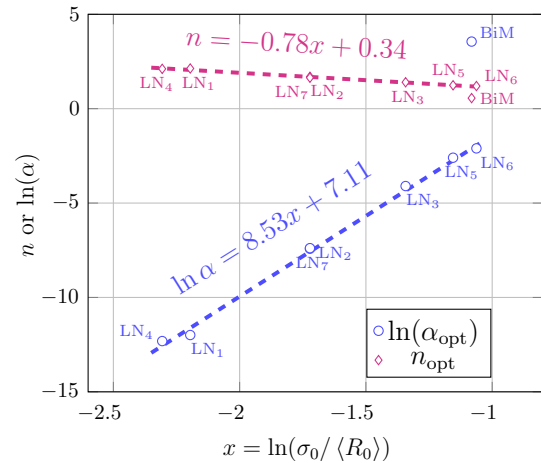


Figure 11 Optimized values α_{opt} and n_{opt} obtained by inverse analysis from the FF simulation results and linear relationships between the set of parameters $(\ln(\alpha); n)$ and the ratio $\ln(\sigma_0 / \langle R_0 \rangle)$.

Inverse analyses were performed in order to obtain optimal values of α_{opt} and n_{opt} which minimize $L_{B\&T}^2$. These values (see Table 3) are plotted in Fig. 11 and the corresponding $L_{B\&T}^2$ are illustrated by red bars in Fig. 8. Interestingly, the results of Table 3 and Fig. 8 show that there exists, for each initial distribution, a set of parameters $(\alpha_{opt}; n_{opt})$ which predicts very accurately the evolution of $\langle R \rangle$, with $L_{B\&T}^2 < 5\%$. Furthermore, the LN₆ initial GSD presents the couple of parameters $(\alpha_{opt}; n_{opt})$ that is closest to the B&T classical parameters ($\alpha = 0.5; n = 1$). This distribution has the largest ratio $(\sigma_0 / \langle R_0 \rangle \simeq 0.35)$ of this study. It is worth noting that increase the ratio $\sigma_0 / \langle R_0 \rangle$ should lead to a new couple of parameters $(\alpha_{opt}; n_{opt})$ even closer to the B&T parameters. In [4], the authors found in 2D a couple parameters $(\alpha_{opt}; n_{opt})$ close to B&T parameters for initial GSDs having a ratio $\sigma_0 / \langle R_0 \rangle \simeq 0.45$.

The predictions of $\langle R \rangle$ obtained by combining Eq. 8 with the set of parameters $(\alpha_{opt}; n_{opt})$ have been plotted in Fig. 9 (dotted curves) for the LN₄ and LN₆ initial GSDs. It is clearly observed that the resulting curves obtained with Eq. 8 (dotted curves) are closer to full field predictions than resulting curves obtained with Eq. 6 (dashed curves). However, the transient regime characterized by a decrease in $\langle R \rangle$ during the first hour of treatment is not well described yet.

It is worth noting that the α_{opt} and the n_{opt} values increase and decrease, respectively, with the $\sigma_0 / \langle R_0 \rangle$ ratio (see Table 3). This trend has already been observed in the study proposed in [4]. These

Table 3 Line 1–2 Optimized B&T model parameters α_{opt} and n_{opt} obtained by inverse analysis from the full field simulation results (see Eq. 6) ; (line 3–4) Fitted mean field model parameters α_{fit} and n_{fit} obtained by using the new formulations of Eq. 9

	LN ₁	LN ₂	LN ₃	LN ₄	LN ₅	LN ₆	LN ₇	BiM
α_{opt}	6.20e-6	6.00e-4	1.66e-2	4.50e-6	7.45e-2	1.22e-1	6.18e-4	35.0
n_{opt}	2.13	1.69	1.37	2.11	1.24	1.20	1.64	0.56
α_{fit}	8.67e-6	5.67e-4	1.22e-2	3.69e-6	7.32e-2	1.58e-1	5.66e-4	1.22e-1
n_{fit}	2.06	1.67	1.39	2.13	1.23	1.16	1.67	1.18
$\ln(\sigma_0/\langle R_0 \rangle)$	-2.20	-1.71	-1.35	-2.30	-1.14	-1.05	-1.71	-1.08

Line 5 Ratio of the initial GSD characteristics

observations confirm that the ratio $\sigma_0/\langle R_0 \rangle$ is relevant for describing the evolution of α and n . Furthermore, the sets of parameters $(\alpha_{opt}; n_{opt})$ are observed to be quasi-identical for the two LN₂ and LN₇ initial GSDs which present the same $\sigma_0/\langle R_0 \rangle$ ratio. By plotting the parameters $\ln(\alpha_{opt})$ and n_{opt} as a function of the ratio $\ln(\sigma_0/\langle R_0 \rangle)$ in Fig. 11, two linear relationships can be deduced for the n and α model parameters:

$$\begin{aligned} \ln(\alpha_{fit}) &= 8.53 \ln\left(\frac{\sigma_0}{\langle R_0 \rangle}\right) + 7.11 \\ n_{fit} &= -0.78 \ln\left(\frac{\sigma_0}{\langle R_0 \rangle}\right) + 0.34, \end{aligned} \tag{9}$$

where these two constant parameters are quite different from those obtained in [4] probably due to the fact that this study is investigated in 3D. Combining Eq. 8 and Eq. 9 results in the following improved B&T formulation:

$$\langle R \rangle^2 - \langle R_0 \rangle^2 = 1224.15 \left(\frac{\sigma_0}{\langle R_0 \rangle}\right)^{8.53} \times M\gamma t^{-0.78 \ln\left(\frac{\sigma_0}{\langle R_0 \rangle}\right) + 0.34} \tag{10}$$

Although the set $(\ln(\alpha) = 3.56; n = 0.56)$ obtained for the BiM initial GSD predicts well the evolution of $\langle R \rangle$, it does not follow the trends obtained for the log-normal initial GSDs (see Fig. 11). So the formulation of the B&T model given by Eq. 10 is only accurate for log-normal initial GSDs. By using Eq. 10, small $L_{B\&T}^2$ are obtained (see beige bars in Fig. 8b). An interesting prospect of this study will be to perform the same analysis for different bimodal distributions.

Conclusion

The present study is devoted to the modeling of ideal grain growth phenomenon. More specifically, the Hillert and B&T grain growth models have been confronted with large full field simulations at the polycrystal scale. These full field simulations are

based on a level set method working within a finite element framework. Eight initial GSDs have been considered for the comparisons.

The Hillert model is shown to be versatile since it considers the initial GSD of the microstructure. However, this model relies on a first-order parameter β which needs to be finely calibrated. Numerical full field investigations have highlighted a new value for β , which is globally constant around 1.4 for all initial distributions. We have finally demonstrated that the calibrated Hillert model predicts finely $\langle R \rangle$ and the evolution of the distribution curves, even for the BiM distribution.

The classical B&T model does not take into account the initial GSD, which makes it inaccurate in many cases. Based on full field simulation results, a new B&T formulation given in Eq. 10 has been proposed. This new formulation has been proven to be able to predict accurately the evolution of $\langle R \rangle$ for any log-normal initial GSD, regardless of σ_0 and $\langle R_0 \rangle$. On the other hand, this new model is not universal and needs to be improved in order to consider other kinds of initial GSDs, like bimodal distributions.

Future work will be dedicated to (I) discuss the variability of the full field results obtained in comparison with the MacPherson–Srolovitz equation [27], (II) perform additional simulations considering anisotropic grain boundary energy and/or mobility, (III) complete the development of a full field model devoted to dynamic recrystallization, (IV) perform the same kind of analysis in the context of the static and dynamic recrystallization phenomena, and (V) perform experimental measurements to be compared with the newly proposed mean field formulations.

Compliance with ethical standards

Conflict of Interest The authors declare that they have no conflict of interest.

References

- [1] Fatima Vaz M, Fortes M (1988) Grain size distribution: the lognormal and the gamma distribution functions. *Scripta Metall* 22(1):35–40. doi:[10.1016/S0036-9748\(88\)80302-8](https://doi.org/10.1016/S0036-9748(88)80302-8)
- [2] Raecisina B, Sinclair CW (2009) A representative grain size for the mechanical response of polycrystals. *Mater Sci Eng A* 525(1–2):78–82. doi:[10.1016/j.msea.2009.06.045](https://doi.org/10.1016/j.msea.2009.06.045)
- [3] Luther T, Könke C (2009) Polycrystal models for the analysis of intergranular crack growth in metallic materials. *Eng Fract Mech* 76(15):2332–2343. doi:[10.1016/j.engfracmech.2009.07.006](https://doi.org/10.1016/j.engfracmech.2009.07.006)
- [4] Cruz-Fabiano A, Logé R, Bernacki M (2014) Assessment of simplified 2D grain growth models from numerical experiments based on a level set framework. *Comput Mater Sci* 92:305–312. doi:[10.1016/j.commatsci.2014.05.060](https://doi.org/10.1016/j.commatsci.2014.05.060)
- [5] Hallberg H (2011) Approaches to modeling of recrystallization. *Metals* 1(1):16–48. doi:[10.3390/met1010016](https://doi.org/10.3390/met1010016)
- [6] Rollett AD, Srolovitz DJ, Anderson MP (1989) Simulation and theory of abnormal grain growth-anisotropic grain boundary energies and mobilities. *Acta Metall* 37(4):1227–1240. doi:[10.1016/0001-6160\(89\)90117-X](https://doi.org/10.1016/0001-6160(89)90117-X)
- [7] Rollett AD, Raabe D (2001) A hybrid model for mesoscopic simulation of recrystallization. *Comput Mater Sci* 21(1):69–78. doi:[10.1016/S0927-0256\(00\)00216-0](https://doi.org/10.1016/S0927-0256(00)00216-0)
- [8] Holm EA, Hassold GN, Miodownik MA (2001) On misorientation distribution evolution during anisotropic grain growth. *Acta Mater* 49(15):2981–2991. doi:[10.1016/S1359-6454\(01\)00207-5](https://doi.org/10.1016/S1359-6454(01)00207-5)
- [9] Raabe D (1999) Introduction of a scalable three-dimensional cellular automaton with a probabilistic switching rule for the discrete mesoscale simulation of recrystallization phenomena. *Philos Magn A* 79(10):2339–2358. doi:[10.1080/01418619908214288](https://doi.org/10.1080/01418619908214288)
- [10] Krill CE, Chen LQ (2002) Computer simulation of 3-D grain growth using a phase-field model. *Acta Mater* 50(12):3059–3075. doi:[10.1016/S1359-6454\(02\)00084-8](https://doi.org/10.1016/S1359-6454(02)00084-8)
- [11] Bernacki M, Chastel Y, Coupez T, Logé R (2008) Level set framework for the numerical modelling of primary recrystallization in polycrystalline materials. *Scr Mater* 58(12):1129–1132. doi:[10.1016/j.scriptamat.2008.02.016](https://doi.org/10.1016/j.scriptamat.2008.02.016)
- [12] Bernacki M, Logé R, Coupez T (2011) Level set framework for the finite-element modelling of recrystallization and grain growth in polycrystalline materials. *Scr Mater* 64(6):525–528. doi:[10.1016/j.scriptamat.2010.11.032](https://doi.org/10.1016/j.scriptamat.2010.11.032)
- [13] Scholtes B, Shakoor M, Settefrati A, Bouchard PO, Bozzolo N, Bernacki M (2015) New finite element developments for the full field modeling of microstructural evolutions using the level-set method. *Comput Mater Sci* 109:388–398. doi:[10.1016/j.commatsci.2015.07.042](https://doi.org/10.1016/j.commatsci.2015.07.042)
- [14] Hallberg H (2013) A modified level set approach to 2D modeling of dynamic recrystallization. *Model Simul Mater Sci Eng* 21(8):085012. doi:[10.1088/0965-0393/21/8/085012](https://doi.org/10.1088/0965-0393/21/8/085012)
- [15] Hillert M (1965) On the theory of normal and abnormal grain growth. *Acta Metall Mater* 13:227. doi:[10.1017/CBO9781107415324.004](https://doi.org/10.1017/CBO9781107415324.004)
- [16] Burke J, Turnbull D (1952) Recrystallization and grain growth. *Prog Met Phys* 3:220–292. doi:[10.1016/0502-8205\(52\)90009-9](https://doi.org/10.1016/0502-8205(52)90009-9)
- [17] Hitti K, Laure P, Coupez T, Silva L, Bernacki M (2012) Precise generation of complex statistical Representative Volume Elements (RVEs) in a finite element context. *Comput Mater Sci* 61:224–238. doi:[10.1016/j.commatsci.2012.04.011](https://doi.org/10.1016/j.commatsci.2012.04.011)
- [18] Hitti K, Bernacki M (2013) Optimized Dropping and Rolling (ODR) method for packing of poly-disperse spheres. *Appl Math Model* 37(8):5715–5722. doi:[10.1016/j.apm.2012.11.018](https://doi.org/10.1016/j.apm.2012.11.018)
- [19] El Wahabi M, Cabrera J, Prado J (2003) Hot working of two AISI 304 steels: a comparative study. *Mater Sci Eng A* 343(1–2):116–125. doi:[10.1016/S0921-5093\(02\)00357-X](https://doi.org/10.1016/S0921-5093(02)00357-X)
- [20] Scholtes B, Boulais-sinou R, Settefrati A, Pino Muñoz D, Poitault I, Montouchet A, Bozzolo N, Bernacki M (2016) 3D level set modeling of static recrystallization considering stored energy fields. *Comput Mater Sci* 122:57–71. doi:[10.1016/j.commatsci.2016.04.045](https://doi.org/10.1016/j.commatsci.2016.04.045)
- [21] Darvishi Kamachali R, Steinbach I (2012) 3-D phase-field simulation of grain growth: topological analysis versus mean-field approximations. *Acta Mater* 60(6–7):2719–2728. doi:[10.1016/j.actamat.2012.01.037](https://doi.org/10.1016/j.actamat.2012.01.037)
- [22] Darvishi Kamachali R, Abbondandolo A, Siburg KF, Steinbach I (2015) Geometrical grounds of mean field solutions for normal grain growth. *Acta Mater* 90:252–258. doi:[10.1016/j.actamat.2015.02.025](https://doi.org/10.1016/j.actamat.2015.02.025)
- [23] Suwa Y, Saito Y, Onodera H (2008) Parallel computer simulation of three-dimensional grain growth using the multi-phase-field model. *Mater Trans* 49(4):704–709. doi:[10.2320/matertrans.MRA2007225](https://doi.org/10.2320/matertrans.MRA2007225)
- [24] Rios PR, Dalpian TG, Brandao VS, Castro JA, Oliveira ACL (2006) Comparison of analytical grain size distributions with three-dimensional computer simulations and experimental data. *Scr Mater* 54(9):1633–1637. doi:[10.1016/j.scriptamat.2006.01.007](https://doi.org/10.1016/j.scriptamat.2006.01.007)
- [25] Chao W, Guoquan LIU (2004) Reanalysis of the 3D quasi-stationary grain size distribution based on Hillert grain growth rate equation. *Ser E Technol Sci* 47(1):112–120
- [26] Petch N (1953) The cleavage strength of polycrystals. *J Iron Steel Inst* 174:25
- [27] MacPherson RD, Srolovitz DJ (2007) The von Neumann relation generalized to coarsening of three-dimensional microstructures. *Nature* 446(7139):1053–1055. doi:[10.1038/nature05745](https://doi.org/10.1038/nature05745)